Sensors & Actuators: B. Chemical 333 (2021) 129554

Contents lists available at ScienceDirect

Sensors and Actuators: B. Chemical

journal homepage: www.elsevier.com/locate/snb

Six-in-one peptide functionalized upconversion@polydopamine nanoparticle-based ratiometric fluorescence sensing platform for real-time evaluating anticancer efficacy through monitoring caspase-3 activity

Lin Liu [a,b], Xiaotong Li [b,c], Hua Zhang [b,*], Hongda Chen [b,c], Murad M.A. Abualrejal [b,c], Daqian Song [a,*], Zhenxin Wang [b,c]

[a] College of Chemistry, Jilin University, Changchun, 130012, PR China
[b] State Key Laboratory of Electroanalytical Chemistry, Changchun Institute of Applied Chemistry, Chinese Academy of Sciences, Changchun, 130022, PR China
[c] School of Applied Chemical Engineering, University of Science and Technology of China, Road Baohe District, Hefei, Anhui, 230026, PR China

ARTICLE INFO

Keywords:
Multifunctional nanoparticles
Fluorescence resonance energy transfer
Caspase-3 activity
Anticancer efficacy of photothermal-chemotherapy

ABSTRACT

Herein, a six-in-one peptide functionalized upconversion@polydopamine nanoparticle-based ratiometric fluorescence sensing platform (termed as UCNP@PDA@Cy3-pep) has been fabricated for monitoring the anticancer efficacy of photothermal-chemotherapy in real time through detection of caspase-3 activity. In this work, the upconversion nanoparticle (UCNP) core of UCNP@PDA was employed as an internal reference, while the PDA shell of UCNP@PDA was used as an acceptor of fluorescence resonance energy transfer (FRET) system, photothermal therapy (PTT) agent, loading agent of chemical drug and immobilization platform of Cy3 (donor of FRET) labeled peptide (Cy3-pep), which contains a specific caspase-3 substrate (DEVD) and active tumor-targeting motif (PSP). In the presence of caspase-3, the FRET system was broken through the enzymatic cleavage of DEVD, resulting in a recovery of Cy3 fluorescence emission. Under the optimal conditions, the ratio of recovered Cy3 fluorescence intensity with upconversion luminescent (UCL) intensity was linearly dependent on the caspase-3 concentration within the range of 0.5–50 ng mL^{-1} and the limit of detection (LOD) was calculated as 0.065 ng mL^{-1}. Using mouse-bearing MG-63 tumor as a model system, the capability of as-proposed UCNP@PDA@Cy3-pep has been successfully demonstrated through a real-time noninvasive evaluation of tumor response to PTT and chemotherapy of staurosporine (STS).

1. Introduction

Tumor response to therapy is a critical issue in daily cancer management. In particular, the capability to monitor noninvasively the anticancer efficacy of treatment in real time that can have a significant effect on the outcome of therapy. Apoptosis, a major form of programmed cell death, is crucial for regulation of physiological circumstances and maintaining homeostasis. The monitoring of apoptosis is of great significance in not only many cytobiology and clinical investigations but also the anticancer efficacy of apoptosis-related therapies [1–3]. Caspases are a family of cysteine-aspartic proteases playing a vital role in cell apoptosis, and their activities have been generally used as the key mediators of apoptosis. Among of the caspases, caspase-3 acts as a typical cellular biomarker in the irreversible process of cell apoptosis [4,5]. Hence, the cellular activity of caspase-3 is considered as one of the most important factors to assess the anticancer efficacy of treatment [6–8]. A variety of fluorescence resonance energy transfer (FRET)-based assays have been reported for monitoring caspase-3 activity with high sensitivity in cancer cells [9–12]. However, most of these FRET-based assays are usually employed single functional probe only capable of caspase-3 activity detection, which may cause receiving signal delay due to the different distributions of detection probe and drug [13,14]. A smart sensing platform integrates antitumor therapy and caspase-3 activity detection, which enables to real-time evaluate the outcome of therapy activity in the tumor. Benefit from the rapid development of nanotechnology, nanoparticles/nanocomposites have been used to integrate molecular imaging and therapeutic capabilities into single systems (also known as theranostics) [15–17]. Because of their high tumor accumulation ability, active tumor-targeting nanoparticles can further improve the diagnosis and treatment effect of

* Corresponding authors.
E-mail addresses: zhanghua@ciac.ac.cn (H. Zhang), songdq@jlu.edu.cn (D. Song).

https://doi.org/10.1016/j.snb.2021.129554
Received 8 November 2020; Received in revised form 15 January 2021; Accepted 21 January 2021
Available online 26 January 2021

tumor [18,19]. Although it has been made great progress in development of theranostics, integration of multiple functionalities in one system for real-time monitoring noninvasively anticancer efficacy is still an enormous challenge in bioanalysis and nanomedicines.

Photothermal therapy (PTT) has been identified as a noninvasive method for tumor therapeutic due to its precise spatial-temporal selectivity using conductive particles and minimum side effects on paracarcinoma tissues [20,21]. Detailed researches of molecular mechanism confirmed that the photothermal treatments induce cell death by a programmed apoptosis through a mitochondria-mediated caspase-3 activation pathway [22–24]. In addition, it is demonstrated that the synergistic interaction between PTT and CT can improve significantly the outcome of antitumor. However, there are currently few sensing systems with the ability to real-time self-monitor the synergistic anticancer activity of PTT and chemotherapy in vivo.

The lanthanide-doped upconversion nanoparticles (UCNPs) have been widely used in biomedical imaging because their special photochemical properties, including robust photostability, minimal autofluorescence backgrounds and deep-tissue excitability under near-infrared (NIR) excitation, etc [25–30]. As a bioinspired polymer, polydopamine (PDA) has been demonstrated as not only an excellent PTT agent but also an efficient carrier for loading aromatic chemotherapy drugs because it exhibits good biocompatibility and biodegradability [31], strong NIR absorbance [32], and larger surface area with plenty of functional groups [33]. The PDA can also be used as an efficient acceptor of FRET system since it has strong fluorescence quenching capacity [34–36] combine the advantages of PDA and UCNPs, which have attracted wide interest for diverse applications in bioanalytical and biomedical fields [37,38].

Herein, we developed a six-in-one peptide-functionalized UCNP@PDA-based fluorescent turn-on ratiometric sensing platform (termed as UCNP@PDA@Cy3-pep) for in situ evaluating noninvasively therapeutic efficacy of PTT and chemotherapy through monitoring caspase-3 activity in vitro and in vivo. The six-in-one sensing platform allows the implementation of the following functions: (i) the UCNP core was employed as an internal reference for UCL imaging. (ii) The FRET occurred between the PDA shell and Cy3. (iii) With the specific recognition site DEVD in the peptide, the sensing platform can be used to detect caspase-3. (iv) The tumor-targeting ability was further improved by the PSP motif in the peptide besides the EPR effect of nanoparticles. (v) PDA was used as the photothermal therapy (PTT) agent. (vi) The loaded chemical drug (STS) was used as the chemotherapy agent. In the proof-of-principle, UCNP@PDA@Cy3-pep was used to study the tumor response to the PDA loaded STS (a clinical anticancer drug, see Fig. S1 in Supplementary information (SI) for molecular structure) under different conditions by using a mouse-bearing MG-63 tumor model.

2. Experimental section

2.1. Synthesis of Cy3-pep modified UCNP@PDA and STS loaded UCNP@PDA@Cy3-pep

The preparation of $NaErF_4$: Tm^{3+}@$NaYbF_4$@$NaYF_4$: Nd^{3+} UCNPs (termed as Er@Yb@Y) and UCNP@PDA were prepared according to previously reported method [39,40]. For the preparation of UCNP@PDA@Cy3-pep, 0.04 mg Cy3 modified peptides (Cy3-pep, sequence, GGSDEVDRPSP-K(Ac)-C(Cy3)) in 3 mL Tris buffer (TB, 10 mmol L^{-1}, pH 8.5) were reacted with different amounts of the as-prepared UCNP@PDA (0.1, 0.2, 0.5, 1 and 2 mg), respectively. After stirred vigorously in the dark at 25 °C for 12 h, UCNP@PDA@Cy3-pep were centrifuged repeatedly at 8000 rpm and redispersed in water. For loading STS, the UCNP@PDA@Cy3-pep (1 mg) were dispersed in 5 mL TB and mixed with 2.5 mg mL^{-1} STS in dimethyl sulfoxide solution (DMSO). After stirred vigorously for 20 h, the final products were centrifuged repeatedly at 8000 rpm and dissolved in phosphate buffered saline (PBS, 1 mL, pH 7.4). The nanocomposites were named as UCNP@PDA@Cy3-pep@STS. The loading weight of STS (W) onto the nanoparticles is calculated by deducting the STS in the supernatant from initial STS added according to the standard UV–vis curve of STS at the wavelength of 297 nm (i.e., $W = W_{\text{original STS}} - W_{\text{STS in supernatant}}$).

2.2. Sensing application of UCNP@PDA@Cy3-pep in buffer

For caspase-3 detection, UCNP@PDA@Cy3-pep (Yb content: 50 μg mL^{-1}) were incubated with various concentrations of caspase-3 in 500 μL assay buffer (see SI for details) at 37 °C for 1 h. Subsequently, the fluorescence and UCL spectra of the mixture were measured at the excitation wavelengths of 530 nm and 980 nm continuous wave (CW) NIR laser, respectively. To investigate its selectivity, the UCNP@PDA@Cy3-pep were incubated with a series of enzymes and proteins including trypsin, lysozyme, thrombin, caspase-7, caspase-9, and caspase-3 inhibitor (Z-DEVD-FMK) under optimized conditions.

2.3. Detection of caspase-3 activity in MG-63 cells

The MG-63 cells (8×10^3 cells per well) were seeded into 96-well microtiter plate for 24 h. Afterward, the cells were treated with 50 μg mL^{-1} UCNP@PDA@Cy3-pep or UCNP@PDA@Cy3-pep@STS in 100 μL fresh DMEM at 37 °C for another 3 h, and the untreated cells were used as control sample. Then, the cells were irradiated under different laser densities (1.5 and 1.8 W cm^{-2}) for 6 min, and the temperature changes of MG-63 cells were recorded by an infrared thermal camera. The cells were further incubated in darkness at 37 °C for another 4 h and then washed with 100 μL PBS. Finally, the cells were imaged by a reconstructive Nikon Ti-S fluorescent microscope with excitation wavelengths at 530 nm for Cy3 imaging and 980 nm for UCL imaging. For quantitative measurement, UCNP@PDA@Cy3-pep or UCNP@PDA@Cy3-pep@STS stained cells in 48-well plate were irradiated by 808 nm laser which is equipped with a 1 cm beam expander. Then, the cells were detached from the 48-well plate and then centrifuged at 1000 rpm for 5 min and redispersed in 500 μL PBS. In addition, the cells treated with 100 μM STS for 4 h were also detached from the 6-well plate and resuspended in 100 μL lysis buffer. Subsequently, the cell lysates containing different cell numbers were incubated with UCNP@PDA@Cy3-pep (Yb content: 50 μg mL^{-1}) in 500 μL assay buffer at 37 °C for 1 h. Then, the fluorescence and UCL spectra of mixture were measured, respectively.

2.4. In vivo apoptosis imaging

All animal experiments were conformed to the guidelines of the Regional Ethics Committee for Animal Experiments established by Jilin University Institutional Animal Care and Use. Male BALB/c nude mice (4–6 weeks old) were selected for establishing a MG-63 tumor model and inoculated with MG-63 cells on the right flanks of mice. As the tumor volume reached about 60 mm^3, the mice were divided into six treatment groups: (i) UCNP@PDA@Cy3-pep, (ii) UCNP@PDA@Cy3-pep@STS, (iii) UCNP@PDA@Cy3-pep + laser (1.5 W cm^{-2}), (iv) UCNP@PDA@Cy3-pep + laser (1.8 W cm^{-2}), (v) UCNP@PDA@Cy3-pep@STS + laser (1.5 W cm^{-2}), (vi) UCNP@PDA@Cy3-pep@STS + laser (1.8 W cm^{-2}). Then, 1.5 mg mL^{-1} UCNP@PDA@Cy3-pep or UCNP@PDA@Cy3-pep@STS (Yb^{3+} content, 150 μL 0.9 wt% NaCl) were injected intravenously into tumor-bearing mice. The mice were irradiated with an 808 nm laser at 6 h post-injection and the temperature increases at tumor sites were recorded. Subsequently, the in vivo fluorescence imaging was collected by the Davinch Invivo HR imaging system at predetermined time intervals. Meanwhile, the in vivo UCL imaging was also performed at the indicated time points of post-irradiation on a home-made in vivo imaging system equipped with a 980 nm laser (2.5 W cm^{-2}).

3. Results and discussion

3.1. Construction and characterization of the UCNP@PDA@Cy3-pep

The as-proposed FRET ratiometric sensing platform (illustrated in Scheme 1) was using Cy3 as the energy donor, PDA as the energy acceptor and UCNP as the internal reference. In the absence of caspase-3, the UCNP@PDA@Cy3-pep shows weak fluorescence intensity due to the efficient quenching effect of PDA. In the presence of caspase-3, the FRET system is broken through the cleavage of specific substrate (DEVD), resulting in a recovery of Cy3 fluorescence emission. The recovery of Cy3 fluorescence is dependent on the activity of caspase-3, i.e., the higher activity level of caspase-3 leads to stronger recovery of high fluorescence emission of Cy3. Because there are individual differences in cells and other organisms, the cellular internalization amount and tumor accumulation amount of UCNP@PDA@Cy3-pep exhibit slightly variation between different individuals. For improving detection accuracy of caspase-3 activity, the ratio of recovered Cy3 fluorescence intensity with UCL intensity ($F_R = \Delta F_{Cy3}/I_{UCL654}$. Herein, $\Delta F = F_{Cy3} - F_{0Cy3}$, F_{0Cy3} and F_{Cy3} represent the maximum fluorescence intensities of UCNP@PDA@Cy3-pep solutions before and after cleaved by caspase-3, respectively) was used to determine the caspase-3 activity. The detection strategy can eliminate the effect of UCNP@PDA@Cy3-pep amount on the accuracy of detection result.

The as-prepared UCNPs have bright single-band red emission under 980 nm NIR laser excitation (Fig. S2). The as-synthesized Er (core), Er@Yb (core@shell) and Er@Yb@Y (core@shell@shell) UCNPs have uniform size with mean sizes of 21.2 ± 1.9, 26.6 ± 1.7 and 33.3 ± 2.1 nm in diameters, respectively (as shown in Fig. S3). After coated by PDA shell with the thickness of 8 nm, the average size of UCNP@PDA reaches 49.8 ± 2.5 nm in diameters. The XRD patterns of three kinds of UCNPs are all indexed exactly to pure hexagonal phase of β-$NaErF_4$ (JCPDS NO. 27–0689, as shown in Fig. S4). XPS measurement results in Fig. S5 clearly show the presence of the element of Yb in Er@Yb and the element of Nd in Er@Yb@Nd, which indicates the successful synthesis of the core@shell@shell nanoparticles.

The as-prepared UCNP@PDA were further modified by Cy3-pep, which contains a specific cleavable site (DEVD) against caspase-3 and active tumor-targeting site (PSP) [41,42]. As shown in Fig. S6, after the conjugation of Cy3-pep with UCNP@PDA, the maximum absorption peak of Cy3 is red-shifted from 544 nm to 556 nm, indicating the strong interaction between Cy3 and PDA. In addition, the UCNP@PDA@Cy3-pep shows obvious absorption at 808 nm, suggesting the great potential of UCNP@PDA@Cy3-pep for photothermal treatment. XPS measurement result in Fig. S7 clearly shows the presence of element Cl in UCNP@PDA@Cy3-pep, which confirms the successful surface modification of Cy3-pep. As shown in Fig. 1a, the quenching ratio of Cy3 ($F_{QR} = \Delta F_1/F_{added\ (Cy3)}$. Herein, $\Delta F_1 = F_{added\ (Cy3)} - F_{supernatant}$, $F_{added\ (Cy3)}$ means the maximum fluorescence intensity of added Cy3-pep solution and $F_{supernatant}$ means the maximum fluorescence intensity of supernatant after conjugation of Cy3-pep with PDA) is increased with increasing the mass ratio of UCNP@PDA to Cy3-pep (R_m) and reaches c.a. 0.95 when the R_m is more than 25. Therefore, all of the following used UCNP@PDA@Cy3-pep were synthesized at R_m of 25. The TGA analysis indicates the weight loss of UCNP@PDA@Cy3-pep is 7.2% more than that of UCNP@PDA, demonstrating the successful surface coating of Cy3-pep (Fig. S8). The increasing hydrodynamic diameters (HDs) of UCNP@PDA@Cy3-pep also verify the successful surface modification of Cy3-pep (Table S2). After conjugation of Cy3-pep with UCNP@PDA, the fluorescence of Cy3 is significantly quenched (Fig. S9a), while the UCL intensity of UCNP shows negligible change (as shown in Fig. S2b). Furthermore, about 294 Cy3-peptide molecules were immobilized on one UCNP@PDA NP according to the standard calibration curve of Cy3-pep (Fig. S9). Upon 808 nm NIR laser irradiation, UCNP@PDA@Cy3-pep could effectively convert light energy to thermal energy with a monotonical increase of solution temperature in a

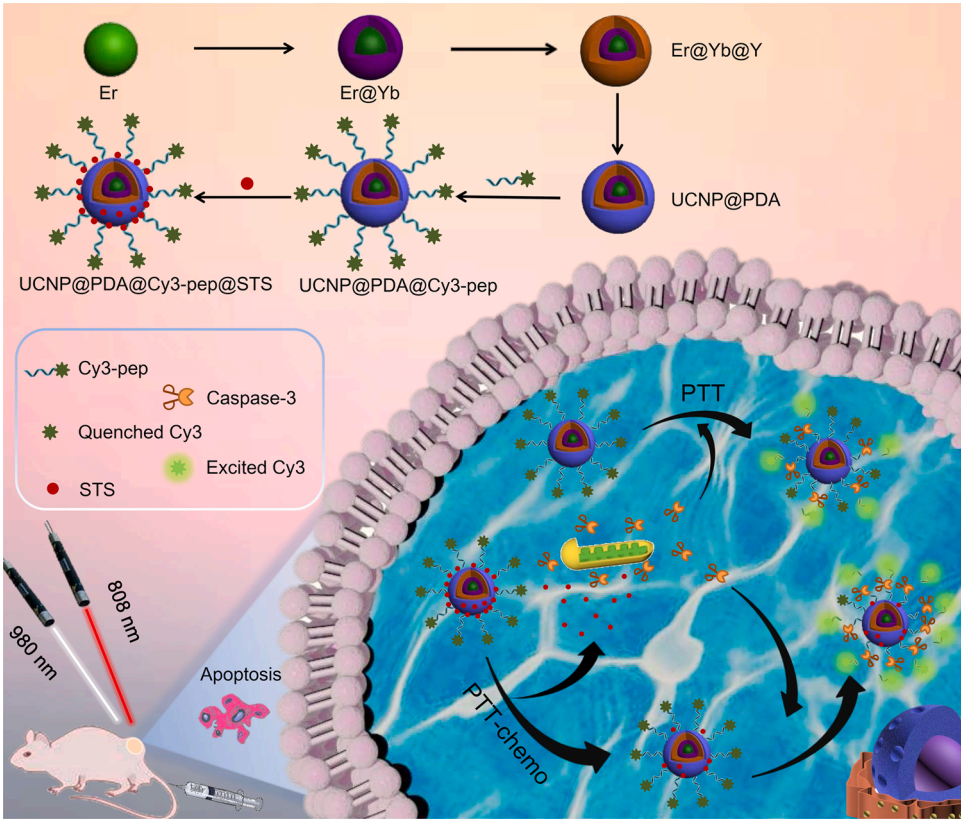

Scheme 1. The schematic illustration of UCNP@PDA@Cy3-pep-based FRET sensing platform for in situ activation and real-time monitoring caspase-3 activity.

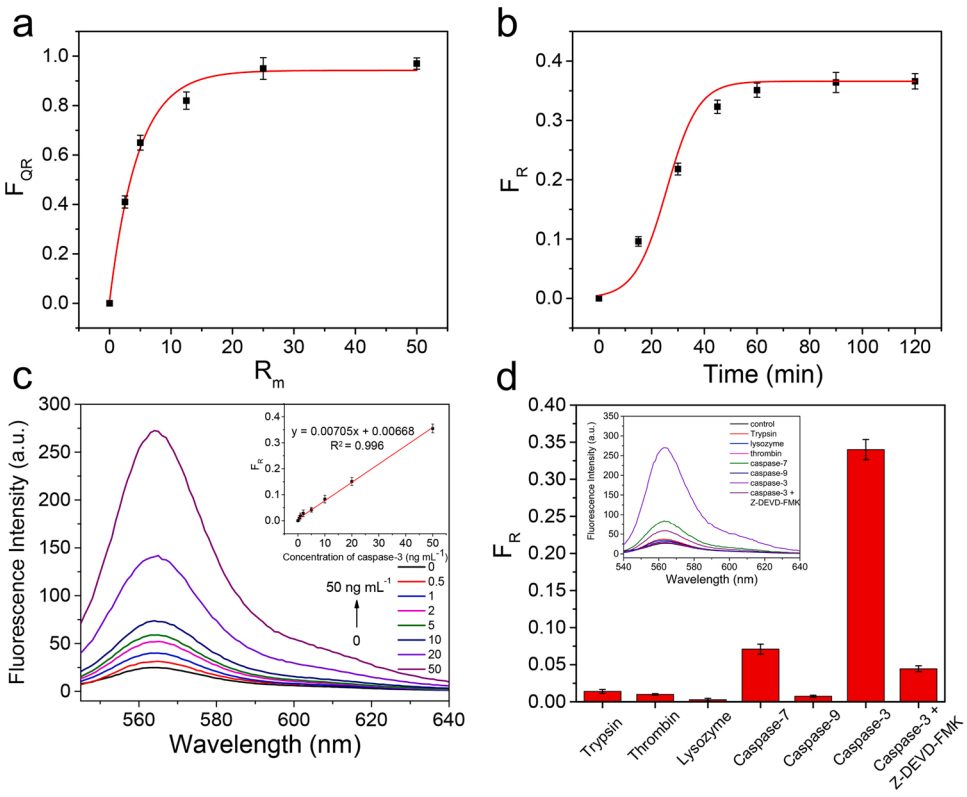

Fig. 1. (a) The F_{QR} curves of Cy3-pep conjugates at different R_m. (b) The F_R of UCNP@PDA@Cy3-pep treated with 50 ng mL^{-1} caspase-3 at various incubation times. (c) Fluorescence spectra of UCNP@PDA@Cy3-pep treated with various concentrations of caspase-3. The inset is the corresponding calibration curve of F_R versus caspase-3 concentration. (d) The selectivity of the UCNP@PDA@Cy3-pep. The inset is the corresponding fluorescence spectra. The error bars mean standard deviations (n = 3).

concentration-dependent or laser density-dependent manner (as shown in Fig. S10). Among these laser densities, 1.5 and 1.8 W cm^{-2} were selected for the follow experiments (Fig. 2a). The UCNP@PDA@Cy3-pep has reasonable photothermal conversion efficiency (η = 21.8 %) and photothermal stability (as shown in Figs. S10c, d, S11, S12). Furthermore, there are negligible effects on the reaction efficiency of UCNP@PDA@Cy3-pep and UCNP@PDA@Cy3-pep@STS with caspase-3 after irradiated by 808 nm laser for 10 min (as shown in Figs. S14, S15). The experimental results suggest that UCNP@PDA@Cy3-pep is not only an excellent sensing platform for detection of caspase-3, but also an ideal agent for PTT. In order to achieve photothermal-chemotherapy, a clinical chemotherapy drug, STS was further loaded on the UCNP@PDA surface. The STS loading efficiency of UCNP@PDA@Cy3-pep is determined to be about 0.93 mg STS/mg UCNP@PDA@Cy3-pep. The high loading capacity could be attributed to the strong intermolecular interactions (such as π–π stacking interaction and hydrogen bond) between STS and PDA. The characteristic peak of STS is red-shifted from 295 nm to 298 nm, indicating the successful loading of STS (Fig. S16). Due to the protonation of amino groups in the STS molecules, the Zeta potential of STS loaded UCNP@PDA@Cy3-pep (termed as UCNP@PDA@Cy3-pep@STS) is higher than that of UCNP@PDA@Cy3-pep (Table S1). Simultaneously, the increasing HDs of UCNP@PDA@Cy3-pep@STS further prove the successful loading of STS (as shown in Table S2). In addition, UCNP@PDA@Cy3-pep@STS has the same UCL and fluorescence properties as those of UCNP@PDA@Cy3-pep (as shown Figs. S2b and S17). The drug releasing behaviors of UCNP@PDA@Cy3-pep@STS were investigated under various solution with different pH values (5.0, 6.5 and 7.4). The STS release efficiency is increased by decreasing the pH value (Fig. S18a). Once the nanocomposites were irradiated with an 808 nm laser, a burst release of STS about 2.5% was observed from UCNP@PDA@Cy3-pep@STS at pH 6.5 (Fig. 2b), while 3.1% was

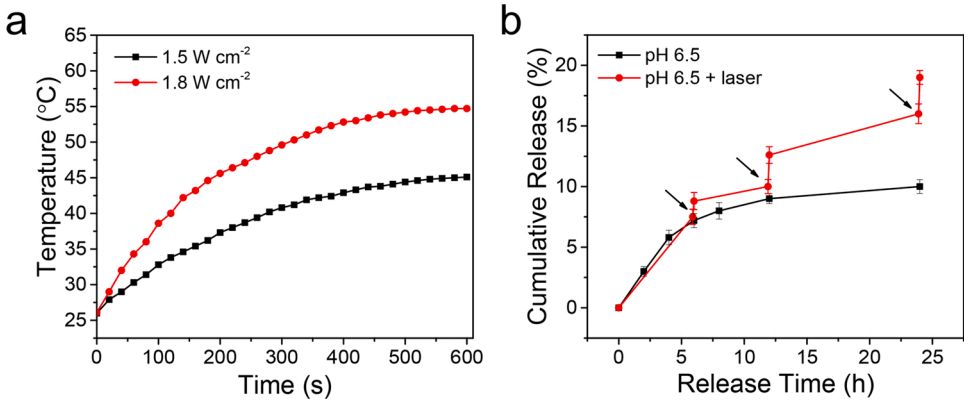

Fig. 2. (a) The solution temperature curves of UCNP@PDA@Cy3-pep aqueous solution (100 μg mL^{-1}) irradiated by an 808 nm laser with 1.5 and 1.8 W cm^{-2}, respectively. (b) Release profiles of STS from UCNP@PDA@Cy3-pep@STS at pH 6.5 with or without 808 nm laser irradiation (1.8 W cm^{-2}) at predetermined time points indicated by arrows.

observed from UCNP@PDA@Cy3-pep@STS at pH 5.0 (Fig. S18b). The pH-dependent and NIR-responsive release behaviors could be used to accelerate the intracellular drug release under certain circumstances.

3.2. Sensing performance of UCNP@PDA@Cy3-pep in buffer

The F_R is gradually increased as the reaction time prolonged and reaches saturation at approximately 60 min (Fig. 1b). The result suggests that UCNP@PDA@Cy3-pep has relatively rapid response time. The fluorescence intensity of Cy3 is proportionally increased with the increase of caspase-3 concentration (as shown in Fig. 1c). After incubation with caspase-3 for 60 min, the UCL spectra of UCNP@PDA@Cy3-pep show negligible change (Fig. S13). There is a good linear correlation between the F_R and caspase-3 concentrations within the range of 0.5–50 ng mL^{-1} with the LOD of 0.065 ng mL^{-1} (S/N = 3), which is comparable to or better than those of reported assays [43–45]. In addition, the sensing capability of UCNP@PDA@Cy3-pep@STS were also examined through detecting the caspase-3 activity. The sensing performance of UCNP@PDA@Cy3-pep@STS (i.e., linear range (0.5–50 ng mL^{-1}) and LOD (0.073 ng mL^{-1})) is similar to that of UCNP@PDA@Cy3-pep, indicating that caspase-3 response of UCNP@PDA@Cy3-pep is not affected by STS loading (as shown in Fig. S17). To test its selectivity, UCNP@PDA@Cy3-pep was treated with other enzymes and proteins, including trypsin, lysozyme, thrombin, caspase-7, caspase-9, and caspase-3 plus inhibitor (Z-DEVD-FMK). UCNP@PDA@Cy3-pep displays the strongest response against the caspase-3 among these analytes (as shown in Fig. 1d). Although caspase-7 can also recognize and cleave the peptide containing DEVD site [46,47], the F_R of UCNP@PDA@Cy3-pep cleaved by caspase-3 is about 4-fold higher than that of UCNP@PDA@Cy3-pep cleaved by caspase-7. In the presence of Z-DEVD-FMK, it is noteworthy that the F_R is decreased significantly. The results demonstrate that UCNP@PDA@Cy3-pep has reasonable selectivity for detection of caspase-3.

3.3. In vitro cytotoxicity evaluation

Prior to intracellular detection, the cytotoxicity of UCNP@PDA@Cy3-pep and UCNP@PDA@Cy3-pep@STS were examined under different conditions by MTT assay in MG-63 cells. As shown in Fig. S19a, the cell viability of UCNP@PDA@Cy3-pep stained MG-63 cells is still above 95 % when the concentration of the UCNP@PDA@Cy3-pep is up to 100 μg mL^{-1} (Yb content). The UCNP@PDA@Cy3-pep@STS shows apparent cytotoxicity on MG-63 cells, which can be attributed to the STS release under acidic tumor microenvironment. After combined with an 808 nm laser, the cell viabilities of UCNP@PDA@Cy3-pep or UCNP@PDA@Cy3-pep@STS stained MG-63 cells are dropped dramatically, demonstrating a concentration-dependent relationship. Importantly, the cytotoxicity of UCNP@PDA@Cy3-pep@STS is much higher than that of UCNP@PDA@Cy3-pep under the same concentration due to the photothermal enhanced chemotherapeutic treatment outcome of STS at elevated temperatures. This result suggests that UCNP@PDA@Cy3-pep@STS has an outstanding synergistic antitumor effect, which is more efficacious in inducing a high number of apoptotic cancer cells. In addition, the cell viabilities of free STS under various concentrations are shown in Fig. S19b, indicating the prominent anticancer efficiency of STS.

3.4. Intracellular caspase-3 activity detection

For demonstrating their sensing capabilities, the UCNP@PDA@Cy3-pep and UCNP@PDA@Cy3-pep@STS were employed for evaluating response of MG-63 cells to different treatments by real-time monitoring caspase-3 activity. The UCNP@PDA@Cy3-pep and UCNP@PDA@Cy3-pep@STS stained MG-63 cells both exhibit strong red UCL emission (as shown in Fig. 3a–g), indicating the efficient cell uptake of them. As expected, the Cy3 fluorescence signal of cells was strongly dependent on the treatments. As shown in Fig. 3i, the F_R of cells follow the order, UCNP@PDA@Cy3-pep@STS plus 1.8 W cm^{-2} 808 nm laser > UCNP@PDA@Cy3-pep@STS plus 1.5 W cm^{-2} 808 nm laser >UCNP@PDA@Cy3-pep plus 1.8 W cm^{-2} 808 nm laser > UCNP@PDA@Cy3-pep@STS > UCNP@PDA@Cy3-pep plus 1.5 W cm^{-2} 808 nm laser. The result is in accordance with the result of cytotoxicity experiment. The Cy3 fluorescence signal of UCNP@PDA@Cy3-pep@STS stained cells is higher than that of UCNP@PDA@Cy3-pep stained cells because the apoptotic machinery of tumor cells can be activated by STS

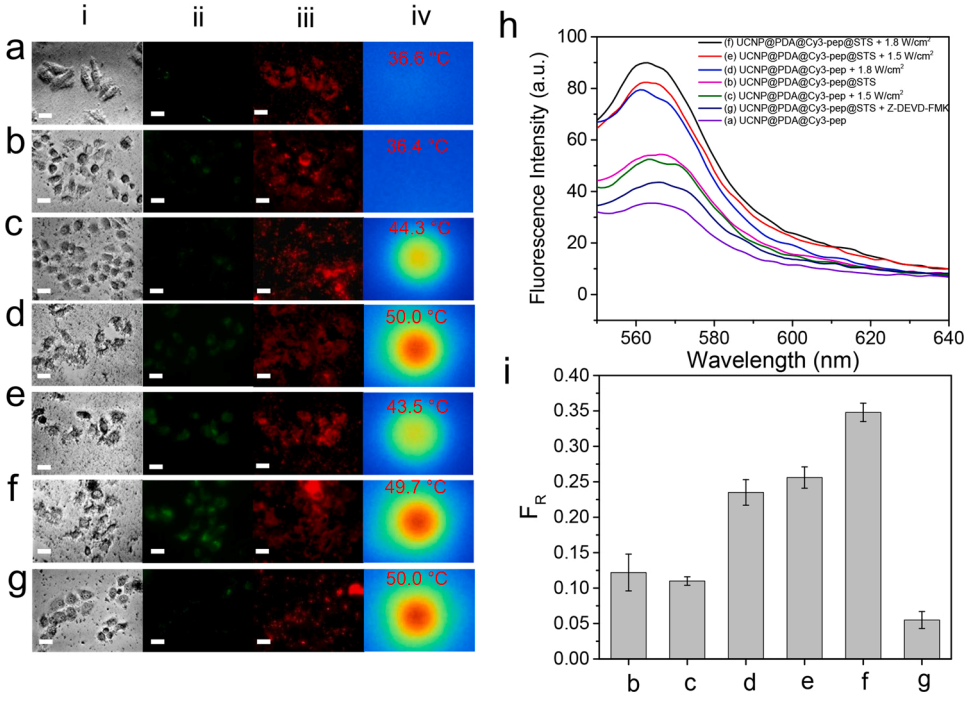

Fig. 3. Fluorescence/UCL imaging of UCNP@PDA@Cy3-pep and UCNP@PDA@Cy3-pep@STS stained MG-63 cells with various treatments. (a) UCNP@PDA@Cy3-pep. (b) UCNP@PDA@Cy3-pep@STS. (c) UCNP@PDA@Cy3-pep plus 808 nm laser (1.5 W cm^{-2}). (d) UCNP@PDA@Cy3-pep plus 808 nm laser (1.8 W cm^{-2}). (e) UCNP@PDA@Cy3-pep@STS plus 808 nm laser (1.5 W cm^{-2}). (f) UCNP@PDA@Cy3-pep@STS plus 808 nm laser (1.8 W cm^{-2}). (g) UCNP@PDA@Cy3-pep@STS plus 808 nm laser (1.8 W cm^{-2}) in the presence of 50 μmol L^{-1} Z-DEVD-FMK before irradiation. Images are obtained from (i) bright-field mode, (ii) Cy3 channel, (iii) UCL channel, (iv) Infrared thermal images of cells with various treatments, respectively. Scale bar: 20 μm. (h) Fluorescence emission spectra of UCNP@PDA@Cy3-pep and UCNP@PDA@Cy3-pep@STS stained MG-63 cells under various treatments. (i) Corresponding F_R of MG-63 cells under various treatments.

[48]. After an 808 nm laser irradiation, the Cy3 fluorescence signals of UCNP@PDA@Cy3-pep/UCNP@PDA@Cy3-pep@STS stained cells exhibited a laser intensity (i.e. temperature-dependent manner)-dependent enhancement, suggesting that the apoptosis rate of tumor cells is increased by increasing the environmental temperature. Under the same laser irradiation conditions, the F_R of UCNP@PDA@Cy3-pep@STS treated cells is higher than that of UCNP@PDA@Cy3-pep treated cells, demonstrating the occurrence of synergistic effect of photothermal-chemotherapy on cell apoptosis. The Cy3 fluorescence of UCNP@PDA@Cy3-pep@STS is decreased dramatically by the Z-DEVD-FMK, implying that the recovery of Cy3 is owing to breaking FRET system through the enzymatic cleavage by caspase-3 (as shown in Fig. 3g). Furthermore, no fluorescence signals are observed in control groups (as shown in Fig. S20).

As shown in Fig. 4, the fluorescence intensity is gradually increased with the increase of MG-63 cell numbers treated by 100 μM STS. And the F_R value of UCNP@PDA@Cy3-pep is linear with the cell numbers within the range of 1×10^3 to 5×10^4 cells with a LOD of 448 cells. The corresponding UCL intensities of UCNP@PDA@Cy3-pep with various numbers of MG-63 cells at 654 nm are shown in Fig. S22. All of the experimental results suggest that UCNP@PDA@Cy3-pep and UCNP@PDA@Cy3-pep@STS could be used to evaluate the therapeutic effect through in situ activation and real-time monitoring of caspase-3 activity level in cancer cells.

3.5. *In vivo caspase-3 activity detection*

A mouse-bearing xenograft MG-63 tumor was used as model for demonstrating the in vivo practicability of UCNP@PDA@Cy3-pep. Prior to in vivo monitoring photothermal-chemotherapy in real time, the toxicity of the UCNP@PDA@Cy3-pep was evaluated by histology analysis and blood test. As shown in Fig. S23, the histology analysis demonstrate that there is neither noticeable tissue damage nor inflammation of UCNP@PDA@Cy3-pep on major organs. There is little difference in blood examination between control mouse and UCNP@PDA@Cy3-pep-treated mouse (Table S3). In addition, no hemolytic phenomenon is observed (Fig. S24). These results indicate that UCNP@PDA@Cy3-pep has good biocompatibility. MG-63 tumor-bearing mice were injected with UCNP@PDA@Cy3-pep and UCNP@PDA@Cy3-pep@STS through tail veins and imaged at different time points, respectively. The maximum UCL intensities of tumor sites were observed at 6 h post-injection(as shown in Fig. S25), indicating the maximum accumulation of nanoparticles in tumor sites. Therefore, the PTT was carried out at 6 h post-injection. Due to the enhanced permeability and retention (EPR) effect and high binding affinity of PSP with tumor cells, UCNP@PDA@Cy3-pep exhibits relatively high accumulation amount (14 %ID g^{-1}) in tumor (as shown in Fig. S26), suggesting that UCNP@PDA@Cy3-pep has high tumor-targeting capacity. This phenomenon helps to improve the detection performance in vivo. The Cy3 fluorescence intensities and F_R of tumor sites are varied with different treatments (as shown in Fig. 5). For instance, no fluorescence signals were observed in control groups (as shown in Fig. S27). Under the same experimental conditions, the F_R of tumor sites in UCNP@PDA@Cy3-pep@STS treated mice (group (v) and (vi)) are higher than those of UCNP@PDA@Cy3-pep treated mice (group (iii) and (iv)). The tumor sites of UCNP@PDA@Cy3-pep treated group (i) exhibit weak Cy3 fluorescence signal, indicating that UCNP@PDA@Cy3-pep has low nonspecific interaction with tumor microenvironment and extremely poor toxicity to cancer cells. The Cy3 fluorescence signals of tumor sites in UCNP@PDA@Cy3-pep@STS treated group (ii) are gradually increased over time, and exhibit 90 % increase in F_R compared with UCNP@PDA@Cy3-pep treated group (i) at 4 h. The results confirm that STS were efficiently released from UCNP@PDA@Cy3-pep@STS under acidic tumor microenvironment, leading to activate caspase-3 mediated apoptosis. After 808 nm laser irradiation, the enhanced Cy3 fluorescence signals of tumor sites are observed in both UCNP@PDA@Cy3-pep treated mice (group (iii) and (iv)) and UCNP@PDA@Cy3-pep@STS treated mice (group (v) and (vi)). Generally, Cy3 fluorescence signals exhibit the laser intensity-dependent enhancement, and have peaked at 6 h post-irradiation. For instance, the F_R of tumor sites in UCNP@PDA@Cy3-pep@STS plus 808 nm NIR laser treated mice are 4.1 times (1.5 W cm^{-2}) and 4.5 times (1.8 W cm^{-2}) higher than those of UCNP@PDA@Cy3-pep treated mice, respectively. In particular, the F_R of tumor sites in UCNP@PDA@Cy3-pep@STS treated mice (group (v)) with 1.5 W cm^{-2} 808 nm laser irradiation are higher than those of UCNP@PDA@Cy3-pep treated mice (group (iv)) with 1.8 W cm^{-2} 808 nm laser irradiation, indicating the more effective apoptosis induced by low-temperature (43.5 °C) PTT-chemo synergistic therapy, which is favorable for minimizing tissue damage by hyperthermia. These experimental results demonstrate that the 808 nm laser irradiation can enhance the release of STS from UCNP@PDA@Cy3-pep@STS, and there is strong synergistic effect of the PTT of PDA and chemotherapy of STS.

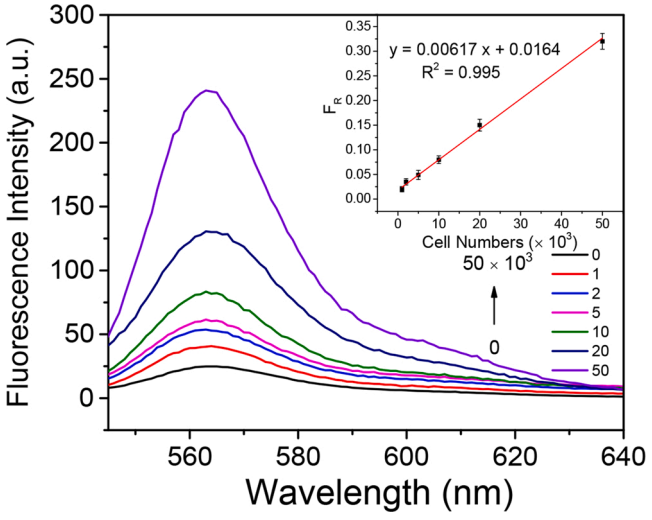

Fig. 4. The fluorescence spectra of UCNP@PDA@Cy3-pep treated with various amounts of MG-63 cells which were treated by 100 μM STS for 4 h. The inset is the corresponding calibration curve of F_R versus cell numbers.

4. Conclusion

In summary, a fluorescence turn-on ratiometric sensing platform has been developed for detection of PTT- and drug-triggered caspase-3 activity in real time through immobilization of caspase-3 cleavable Cy3 modified peptide and loading of anticancer drug on PDA coated UCNP. The results demonstrate that the as-proposed sensing platform has reasonably low LOD for caspase-3 activity detection combined with a large dynamic range. Due to building multiple functionalities in a single nanoparticle, the as-proposed sensing platform can effectively capture the temporal apoptosis process. All of the experimental results unequivocally confirm that the sensing platform can be served as an ideal tool for real-time noninvasive evaluation of tumor response to different treatment modes including PTT, chemotherapy and photothermal-chemo synergistic therapy.

CRediT authorship contribution statement

Lin Liu: Conceptualization, Methodology, Software, Investigation, Validation, Data curation, Writing - original draft. **Xiaotong Li:** Data curation. **Hua Zhang:** Data curation, Writing - review & editing. **Hongda Chen:** Data curation. **Murad M.A. Abualrejal:** Software, Validation. **Daqian Song:** Supervision. **Zhenxin Wang:** Writing - review & editing.

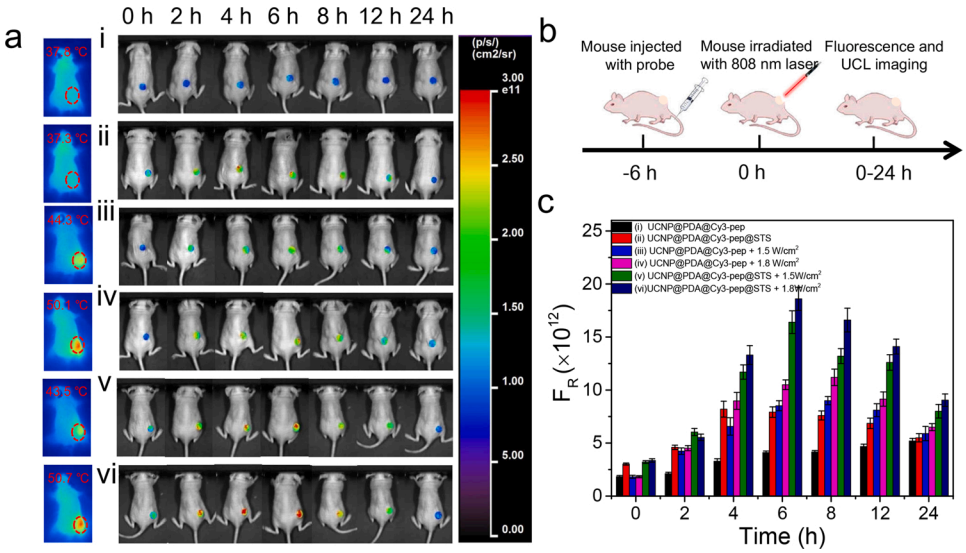

Fig. 5. (a) In vivo fluorescence images of tumor-bearing mice under various treatments. (i) UCNP@PDA@Cy3-pep, (ii) UCNP@PDA@Cy3-pep@STS, (iii) UCNP@PDA@Cy3-pep plus 808 nm laser (1.5 W cm^{-2}), (iv) UCNP@PDA@Cy3-pep plus 808 nm laser (1.8 W cm^{-2}), (v) UCNP@PDA@Cy3-pep@STS plus 808 nm laser (1.5 W cm^{-2}), (vi) UCNP@PDA@Cy3-pep@STS plus 808 nm laser (1.8 W cm^{-2}). (b) The mice treatment process. (c) Quantification of F_R at the tumor sites with various treatments.

Declaration of Competing Interest

The authors report no declarations of interest.

Acknowledgement

The authors would like to thank the National Natural Science Foundation of China (Grant nos. 22074052, 21775145 and 61901438) and Science and Technology Developing Foundation of Jilin Province (Grant No. 20200404192YY) for financial support.

Appendix A. Supplementary data

Supplementary material related to this article can be found, in the online version, at doi:https://doi.org/10.1016/j.snb.2021.129554.

References

[1] X. Yin, B. Yang, B.B. Chen, M. He, B. Hu, Multifunctional gold nanocluster decorated metal-organic framework for real-time monitoring of targeted drug delivery and quantitative evaluation of cellular therapeutic response, Anal. Chem. 91 (2019) 10596–10603.
[2] A.C. Clark, Caspase allostery and conformational selection, Chem. Rev. 116 (2016) 6666–6706.
[3] U. Fischer, K. Schulze-Osthoff, New approaches and therapeutics targeting apoptosis in disease, Pharmacol. Rev. 57 (2005) 187–215.
[4] X.N. Gao, J. Li, M.M. Luan, Y.H. Li, W. Pan, N. Li, et al., Real-time in situ monitoring of signal molecules' evolution in apoptotic pathway via Au-Se bond constructed nanoprobe, Biosens. Bioelectron. 147 (2020) 8.
[5] Q.P. Rao, M.D. Yang, G. Liu, J.J. Wang, Y.C. Bu, J. Zhang, et al., Real-time monitoring apoptosis and autophagy among multiple organelles by adjusting the slight structure, Sens. Actuator B-Chem. 302 (2020) 7.
[6] A. Kulkarni, P. Rao, S. Natarajan, A. Goldman, V.S. Sabbisetti, Y. Khater, et al., Reporter nanoparticle that monitors its anticancer efficacy in real time, Proc. Natl. Acad. Sci. U. S. A. 113 (2016) E2104–E2113.
[7] N. Xia, Y.L. Huang, Z.Y. Cui, S.D. Liu, D.H. Deng, L. Liu, et al., Impedimetric biosensor for assay of caspase-3 activity and evaluation of cell apoptosis using self-assembled biotin-phenylalanine network as signal enhancer, Sens. Actuator B-Chem. 320 (2020) 7.
[8] J. Wang, Z.L. Zhou, F. Zhang, H. Xu, W.L. Chen, T.T. Jiang, A novel nanocomposite based on fluorescent turn-on gold nanostars for near-infrared photothermal therapy and self-theranostic caspase-3 imaging of glioblastoma tumor cell, Colloid Surf, B-Biointerfaces 170 (2018) 303–311.
[9] X.L. Huang, M. Swierczewska, K.Y. Choi, L. Zhu, A. Bhirde, J. Park, et al., Multiplex imaging of an intracellular proteolytic cascade by using a broad-spectrum nanoquencher, Angew. Chem.-Int. Edit. 51 (2012) 1625–1630.
[10] D. Feng, F. Tian, W. Qin, X. Qian, A dual-functional lanthanide nanoprobe for both living cell imaging and ICP-MS quantification of active protease, Chem. Sci. 7 (2016) 2246–2250.
[11] Y.L. Tong, X.T. Huang, M. Lu, B.Y. Yu, J.W. Tian, Prediction of drug-induced nephrotoxicity with a hydroxyl radical and caspase light-up dual-signal nanoprobe, Anal. Chem. 90 (2018) 3556–3562.
[12] X. Li, Y.Q. Li, Q. Qiu, Q.R. Wen, Q. Zhang, W.J. Yang, et al., Efficient biofunctionalization of MoS2 nanosheets with peptides as intracellular fluorescent biosensor for sensitive detection of caspase-3 activity, J. Colloid Interface Sci. 543 (2019) 96–105.
[13] Y.Y. Yuan, R.T.K. Kwok, B.Z. Tang, B. Liu, Targeted theranostic platinum(IV) prodrug with a built-in aggregation-induced emission light-up apoptosis sensor for noninvasive early evaluation of its therapeutic responses in situ, J. Am. Chem. Soc. 136 (2014) 2546–2554.
[14] R. Kumar, W.S. Shin, K. Sunwoo, W.Y. Kim, S. Koo, S. Bhuniya, et al., Small conjugate-based theranostic agents: an encouraging approach for cancer therapy, Chem. Soc. Rev. 44 (2015) 6670–6683.
[15] J.J. Zhang, L.L. Ning, J.G. Huang, C. Zhang, K.Y. Pu, Activatable molecular agents for cancer theranostics, Chem. Sci. 11 (2020) 618–630.
[16] M.Y. Zhao, B.H. Li, Y.F. Wu, H.S. He, X.Y. Zhu, H.X. Zhang, et al., A tumor-microenvironment-responsive lanthanide-cyanine FRET sensor for NIR-II luminescence-lifetime in situ imaging of hepatocellular carcinoma, Adv. Mater. 32 (2020) 7.
[17] S.F. Wang, L. Liu, Y. Fan, A.M. El-Toni, M.S. Alhoshan, D.D. Li, et al., In vivo high-resolution ratiometric fluorescence imaging of inflammation using NIR-II nanoprobes with 1550 nm emission, Nano Lett. 19 (2019) 2418–2427.
[18] F.Y. Liu, X.X. He, L. Liu, H.P. You, H.M. Zhang, Z.X. Wang, Conjugation of NaGdF4 upconverting nanoparticles on silica nanospheres as contrast agents for multi-modality imaging, Biomaterials 34 (2013) 5218–5225.
[19] L. Zhou, R. Wang, C. Yao, X.M. Li, C.L. Wang, X.Y. Zhang, et al., Single-band upconversion nanoprobes for multiplexed simultaneous in situ molecular mapping of cancer biomarkers, Nat. Commun. 6 (2015) 6938.
[20] J.W. Lee, H. Jung, H.H. Cho, J.H. Lee, Y. Nam, Gold nanostar-mediated neural activity control using plasmonic photothermal effects, Biomaterials 153 (2018) 59–69.
[21] A. Neira-Carrillo, E. Yslas, Y.A. Marini, P. Vasquez-Quitral, M. Sanchez, A. Riveros, et al., Hybrid biomaterials based on calcium carbonate and polyaniline nanoparticles for application in photothermal therapy, Colloid Surf. B-Biointerfaces 145 (2016) 634–642.
[22] M.R.K. Ali, H.R. Ali, C.R. Rankin, M.A. El-Sayed, Targeting heat shock protein 70 using gold nanorods enhances cancer cell apoptosis in low dose plasmonic photothermal therapy, Biomaterials 102 (2016) 1–8.
[23] Y. Yang, W.J. Zhu, Z.L. Dong, Y. Chao, L. Xu, M.W. Chen, et al., 1D coordination polymer nanofibers for low-temperature photothermal therapy, Adv. Mater. 29 (2017) 12.
[24] M. Mirrahimi, V. Hosseini, S.K. Kamrava, N. Attaran, J. Beik, S. Kooranifar, et al., Selective heat generation in cancer cells using a combination of 808nm laser irradiation and the folate-conjugated Fe2O3@Au nanocomplex, Artif. Cell Nanomed. Biotechnol. 46 (2018) S241–S253.
[25] M. Nyk, R. Kumar, T.Y. Ohulchanskyy, E.J. Bergey, P.N. Prasad, High contrast in vitro and in vivo photoluminescence bioimaging using near infrared to near infrared up-conversion in Tm3+ and Yb3+ doped fluoride nanophosphors, Nano Lett. 8 (2008) 3834–3838.
[26] L. Liu, H. Zhang, D.Q. Song, Z.X. Wang, An upconversion nanoparticle-based fluorescence resonance energy transfer system for effectively sensing caspase-3 activity, Analyst 143 (2018) 761–767.
[27] L. Liu, H. Zhang, Z.X. Wang, D.Q. Song, Peptide-functionalized upconversion nanoparticles-based FRET sensing platform for Caspase-9 activity detection in vitro and in vivo, Biosens. Bioelectron. 141 (2019) 7.
[28] Y.T. Zhong, Z.R. Ma, F.F. Wang, X. Wang, Y.J. Yang, Y.L. Liu, et al., In vivo molecular imaging for immunotherapy using ultra-bright near-infrared-IIb rare-earth nanoparticles, Nat. Biotechnol. 37 (2019) 1322–1331.

[29] Y. Fan, P.Y. Wang, Y.Q. Lu, R. Wang, L. Zhou, X.L. Zheng, et al., Lifetime-engineered NIR-II nanoparticles unlock multiplexed in vivo imaging, Nat. Nanotechnol. 13 (2018) 941–946.
[30] R. Wang, X.M. Li, L. Zhou, F. Zhang, Epitaxial seeded growth of rare-earth nanocrystals with efficient 800 nm near-infrared to 1525 nm short-wavelength infrared downconversion photoluminescence for in vivo bioimaging, Angew. Chem.-Int. Edit. 53 (2014) 12086–12090.
[31] Q.L. Fang, J.F. Zhang, L.F. Bai, J.Y. Duan, H.J. Xu, K.C.F. Leung, et al., In situ redox-oxidation polymerization for magnetic core-shell nanostructure with polydopamine-encapsulated-Au hybrid shell, J. Hazard. Mater. 367 (2019) 15–25.
[32] Y.L. Liu, K.L. Ai, J.H. Liu, M. Deng, Y.Y. He, L.H. Lu, Dopamine-melanin colloidal nanospheres: an efficient near-infrared photothermal therapeutic agent for in vivo cancer therapy, Adv. Mater. 25 (2013) 1353–1359.
[33] B.H. Kim, D.H. Lee, J.Y. Kim, D.O. Shin, H.Y. Jeong, S. Hong, et al., Mussel-inspired block copolymer lithography for low surface energy materials of teflon, graphene, and gold, Adv. Mater. 23 (2011) 5618–5622.
[34] X.S. Liu, J.M. Cao, H. Li, J.Y. Li, Q. Jin, K.F. Ren, et al., Mussel-inspired polydopamine: a biocompatible and ultrastable coating for nanoparticles in vivo, ACS Nano 7 (2013) 9384–9395.
[35] L. Ma, F.Y. Liu, Z. Lei, Z.X. Wang, A novel upconversion@polydopamine core@shell nanoparticle based aptameric biosensor for biosensing and imaging of cytochrome c inside living cells, Biosens. Bioelectron. 87 (2017) 638–645.
[36] W.B. Qiang, W. Li, X.Q. Li, X. Chen, D.K. Xu, Bioinspired polydopamine nanospheres: a superquencher for fluorescence sensing of biomolecules, Chem. Sci. 5 (2014) 3018–3024.
[37] Y. Dai, D.P. Yang, D.P. Yu, C. Cao, Q.H. Wang, S.H. Xie, et al., Mussel-inspired polydopamine-coated lanthanide nanoparticles for NIR-II/CT dual imaging and photothermal therapy, ACS Appl. Mater. Interfaces 9 (2017) 26674–26683.
[38] B. Liu, C.X. Li, B.G. Xing, P.P. Yang, J. Lin, Multifunctional UCNPs@PDA-ICG nanocomposites for upconversion imaging and combined photothermal/photodynamic therapy with enhanced antitumor efficacy, J. Mater. Chem. B 4 (2016) 4884–4894.
[39] R.R. Tian, S. Zhao, G.F. Liu, H.D. Chen, L.N. Ma, H.P. You, et al., Construction of lanthanide-doped upconversion nanoparticle-Uelx Europaeus Agglutinin-I bioconjugates with brightness red emission for ultrasensitive in vivo imaging of colorectal tumor, Biomaterials 212 (2019) 64–72.
[40] F.Y. Liu, Q. Zhao, H.P. You, Z.X. Wang, Synthesis of stable carboxy-terminated NaYF4:Yb3+, Er3+@SiO2 nanoparticles with ultrathin shell for biolabeling applications, Nanoscale 5 (2013) 1047–1053.
[41] Y. Li, Y. Lei, E. Wagner, C. Xie, W.Y. Lu, J.H. Zhu, et al., Potent retro-inverso D-peptide for simultaneous targeting of angiogenic blood vasculature and tumor cells, Bioconjugate Chem. 24 (2013) 133–143.
[42] X. Li, Z.X. Xie, C. Xie, W.Y. Lu, C.L. Gao, H.L. Ren, et al., D-SP5 peptide-modified highly branched polyethylenimine for gene therapy of gastric adenocarcinoma, Bioconjugate Chem. 26 (2015) 1494–1503.
[43] P.M. Shih, T.K. Liu, K.T. Tan, Fluorescence amplified detection of proteases by the catalytic activation of a semisynthetic sensor, Chem. Commun. 49 (2013) 6212–6214.
[44] H.B. Wang, Q. Zhang, X. Chu, T.T. Chen, J. Ge, R.Q. Yu, Graphene oxide-peptide conjugate as an intracellular protease sensor for caspase-3 activation imaging in live cells, Angew. Chem.-Int. Edit. 50 (2011) 7065–7069.
[45] X.Y. Huang, Y.R. Liang, L.G. Ruan, J.C. Ren, Chemiluminescent detection of cell apoptosis enzyme by gold nanoparticle-based resonance energy transfer assay, Anal. Bioanal. Chem. 406 (2014) 5677–5684.
[46] Y.P. Shi, C.Q. Yi, Z.M. Zhang, H. Zhang, M.J. Li, M.S. Yang, et al., Peptide-bridged assembly of hybrid nanomaterial and its application for caspase-3 detection, ACS Appl. Mater. Interfaces 5 (2013) 6494–6501.
[47] H.B. Shi, R.T.K. Kwok, J.Z. Liu, B.G. Xing, B.Z. Tang, B. Liu, Real-time monitoring of cell apoptosis and drug screening using fluorescent light-up probe with aggregation-induced emission characteristics, J. Am. Chem. Soc. 134 (2012) 17972–17981.
[48] X.J. Liu, X.X. Song, D.R. Luan, B. Hu, K.H. Xu, B. Tang, Real-time in situ visualizing of the sequential activation of caspase cascade using a multicolor gold-selenium bonding fluorescent nanoprobe, Anal. Chem. 91 (2019) 5994–6002.

Lin Liu is currently a Ph.D. student in the College of Chemistry at Jilin University, Her research projects focus on the preparation of novel multifunctional upconversion nanoparticles-based biosensors and their applications in biological detection.

Xiaotong Li is now a graduate student in the University of Science and Technology of China. Her recent research is to use nanosensors to detect disease-related phosphatase activity.

Hua Zhang is an associate professor of Chemistry at Changchun Institute of Applied Chemistry (CIAC), Chinese Academy of Sciences (CAS), and her main research orientation is the application of upconversion nanoparticles in detecting protease activities.

Hongda Chen is currently a Ph.D. student in the University of Science and Technology of China. His research is the application of magnetic nanoparticles for bioimaging and photothermal therapy.

Murad M.A. Abualrejal is currently a Ph.D. student in the University of Science and Technology of China. His research is the preparation of novel upconversion nanoparticles for bioimaging in vivo.

Daqian Song is a professor of chemistry at Jilin University. He received his B.S. degree in 1998 and Ph.D. degree in 2003 both from Jilin University. Then he worked as a lecturer at the College of Chemistry, Jilin University, and was appointed as a professor in 2008. His research focuses on spectral and chromatographic analysis, and the study of on-site rapid detection.

Zhenxin Wang is a Professor of Chemistry at Changchun Institute of Applied Chemistry (CIAC), Chinese Academy of Sciences (CAS). He received his BS degree in Analytical Chemistry from Jilin University, and his MS and PhD degrees in Analytical Chemistry from CIAC, CAS. After his doctoral work, Dr Wang worked as postdoctoral research fellow for five years in United Kingdom. His current research focuses on the development of biosensors/bioassays for bioanalytical and environmental applications by using various nanomaterials including gold nanoparticles, graphenes and upconversion nanoparticles.